Femtosecond versus nanosecond magnetization dynamics in ultrathin ferromagnetic bilayers

Anulekha De [1,*] Christopher Seibel [1,†] Sanjay Ashok,[1] Paul Herrgen [1] Akira Lentfert [1] Laura Scheuer,[1,2] Georg von Freymann [1,3] Philipp Pirro [1] Baerbel Rethfeld [1] and Martin Aeschlimann [1]

[1]*Fachbereich Physik and Landesforschungszentrum OPTIMAS, Rheinland-Pfälzische Technische Universität Kaiserslautern-Landau, 67663 Kaiserslautern, Germany*

[2]*Department of Physics and Astronomy, University of Delaware, Newark, Delaware 19716, USA*

[3]*Fraunhofer Institute for Industrial Mathematics ITWM, 67663 Kaiserslautern, Germany*

(Received 28 April 2025; revised 11 August 2025; accepted 5 September 2025; published 2 October 2025)

We investigate the magnetization dynamics of an ultrathin Co (1.5 nm)/Py (1.5 nm) bilayer system from femtosecond (fs) to nanosecond (ns) timescales. Magnetization dynamics in the fs timescales is characterized as a highly nonequilibrium regime due to an ultrafast reduction of magnetization by laser excitation. On the other hand, the dynamics in the ns timescales is characterized as a close-to-equilibrium regime involving the excitation of coherent magnons. We demonstrate that the interfacial interaction between the Co and Py layers in these two nonequilibrium regimes across the timescales is dynamic and simultaneously influences the magnetization loss in the fs timescales and the magnon dynamics in the ns timescales. On ultrafast (fs) timescales, comparison between time-resolved magneto-optical Kerr effect (TR-MOKE) measurements and temperature-based μT model simulations reveals that the bilayer exhibits demagnetization dynamics intermediate between those of its individual layers. When driven far from equilibrium by ultrashort laser pulse excitation, the magnetization dynamics of the individual Co and Py layers appear to remain decoupled and evolve independently in the initial stages of the ultrafast response. On the other hand, in the ns regime, the two individual layers of the bilayer precess together at the same frequency in a coupled manner as one effective single layer. These results improve our understanding of magnetization dynamics across timescales in ultrathin exchanged-coupled ferromagnetic bilayers and provide valuable insights for the design of high-frequency and energy-efficient spintronic device concepts.

DOI: 10.1103/d7vt-jlkg

I. INTRODUCTION

Ultrafast magnetometry is a cutting edge methodology to study light–matter interactions across timescales ranging from a few attoseconds to several nanoseconds in various material systems. This methodology utilizes light pulses with a typical temporal width of a few femtoseconds that can excite as well as detect the magnetization dynamics in magnetic materials with a high spatiotemporal resolution. The demonstration of ultrafast magnetization dynamics in femtosecond laser irradiated thin nickel films by Beaurepaire *et al.* [1] led to the inception of femtomagnetism. The phenomena of laser-induced magnetization dynamics range from the highly nonequilibrium regime on femtosecond timescales [2–7] to the close to equilibrium regime on picosecond to nanosecond timescales [8,9]. Ultrafast magnetometry is typically used to study femtomagnetism in homogeneous films [1,10,11] as well as nano- and heterostructures [6,12,13]. Nevertheless, a clear understanding of the microscopic mechanisms that underlie this cross-timescale phenomenon as well as the methodologies to investigate them in various material systems are incomplete. A wide range of research has been performed on various ferromagnetic systems to understand the mechanisms that underpin femtomagnetism in subpicosecond timescales. In this context, two primary microscopic mechanisms are proposed to underlie ultrafast demagnetization: local spin-flip scattering (SFS) [3–5,14] and nonlocal spin-transport (ST) [6,7,15] processes. The local SFS mechanisms encompass Elliott–Yafet (EY)-type electron-phonon scattering [5], electron-magnon interactions [14], electron-electron Coulomb scattering [4], and relativistic spin-flip events [3]. Regarding nonlocal spin transport, superdiffusive spin transport has been identified as the predominant mechanism contributing to the rapid loss of magnetization [6,7]. It has also been discussed that ultrafast demagnetization is possibly a cooperative effect of the laser field and the spin-orbit coupling (SOC) of the magnetic material [16]. On the longer timescales (picosecond to nanosecond) the generation of coherent magnons are considered to play a strong role. The signature of magnon generation can be observed as precessional dynamics on the nanosecond timescale, which represents a close-to-equilibrium regime [8,9]. This precession of magnetization is governed by the anisotropic

*Contact author: ade@rptu.de
†Contact author: cseibel@rptu.de

Published by the American Physical Society under the terms of the Creative Commons Attribution 4.0 International license. Further distribution of this work must maintain attribution to the author(s) and the published article's title, journal citation, and DOI.

magnetic properties, precessional frequencies, damping constants of magnetic materials, and other material specific parameters [8,9,17,18].

The microscopic mechanisms underlying the ultrafast quenching of magnetization (in highly nonequilibrium region) and their relation to relaxation of magnetization through precession (in close-to-equilibrium region) is rarely explored. A simultaneous investigation of both the ultrafast demagnetization time and damping of the coherent magnons, along with the correlation between them, could contribute to understand the transition from a highly nonequilibrium to a close-to-equilibrium region [19]. However, despite the considerable insights [9,10,20], the relationship between the two parameters is yet to be unambiguously clarified. A direct proportional relation between demagnetization time and damping would hint at, for instance, local spin–flip scattering being the primary contributor to demagnetization [10,20]. An inverse proportional relation, on the other hand, would support the nonlocal spin-transport as the dominant microscopic mechanism [9].

From a materials perspective, the investigation of this cross-timescale phenomenon has so far predominantly focused on single layer ferromagnet (FM) [10], FM/antiferromagnet (AFM) [21] or FM/topological insulator (TI) [22] bilayers. Some reports also studied the ultrafast demagnetization and switching processes on rare earth-transition metal (RE-TM) alloys and bilayers [23–28]. However, only a very few investigations have been conducted to obtain a unified picture of ultrafast demagnetization and precessional damping in ultrathin FM/FM bilayers [29]. Cobalt/Permalloy ($Co/Ni_{80}Fe_{20}$ or Co/Py) bilayers are one of the commonly studied FM/FM exchange spring material systems [30,31]. The exchange coupling between Co and Py is useful for studying buried magnetic interfaces and exchange effects in conducting structures. Understanding the interfacial effects in such exchange coupled bilayers is crucial to finely tailor their properties. A number of works have focused on the magnetic properties of Co/Py bilayers, which have discussed magnon dynamics in such systems [32–38]. Recently, Zhang *et al.* [29] reported a direct proportional relation between demagnetization time and damping in Co/Ni bilayers. Nevertheless, the existing literature lacks a deeper insight into the timescale-dependent dynamic interfacial effect, as well as a unified picture of ultrafast demagnetization and precessional damping in ultrathin, exchange coupled FM/FM bilayers.

In our work, we report a comparative investigation of the magnetization dynamics of a Co/Py ultrathin bilayer system from femtosecond (fs) to nanosecond (ns) timescales using fs amplified laser pulses in a time-resolved magneto-optical Kerr effect (TR-MOKE) methodology. On ultrashort (fs) timescales, by relating experimental demagnetization to the simulations of magnetization using the temperature-based μT model, we find that the demagnetization profiles of the bilayer is intermediate to that of the individual layers and that the two layers behave nearly independently in a decoupled way when the entire system is in the highly nonequilibrium state caused by ultrashort laser pulse excitation. However, on longer (ns) timescales, well after the laser excitation has subsided and the system has relaxed to near thermal equilibrium, the experimentally measured precession dynamics of the ultrathin bilayer reveals a single precessional (magnon) mode, indicating that the two layers precess together with a same frequency in a coupled manner, when the system is in close-to-equilibrium condition. In addition, we examine the dependence of ultrafast demagnetization time on effective damping in terms of laser fluence and discuss possible mechanisms which could explain the correlation between these two parameters in the ultrathin ferromagnetic bilayer.

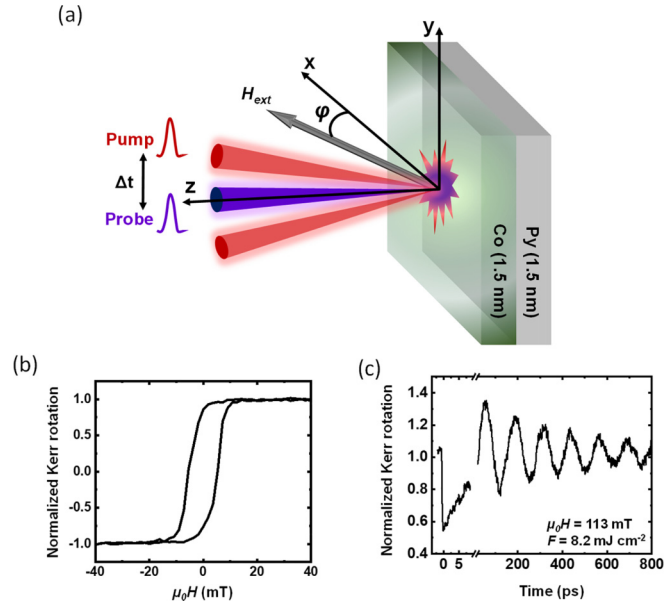


FIG. 1. (a) Schematic of the pump-probe experiment. (b) In-plane hysteresis loop measured by static MOKE. (c) Representative time-resolved data measured at $\mu_0 H = 113$ mT and $F = 8.2$ mJ cm^{-2}.

This paper is structured as follows. Section II describes the material system and its fabrication as well the theoretical and experimental methodologies of investigation. Section III discusses the ultrafast demagnetization dynamics in the highly nonequilibrium regime, precession dynamics in close-to-equilibrium regime and correlation between ultrafast demagnetization time and effective damping of the ultrathin bilayer. Finally, Sec. IV summarizes and concludes.

II. MATERIALS AND METHODS

A Co/Py bilayer film is epitaxially grown on an MgO substrate by molecular beam epitaxy (MBE) in an ultrahigh vacuum chamber. The thickness of the Co and Py layers is 1.5 nm each. The sample is capped with 3 nm Al_2O_3 and 3 nm of Au to protect it from environmental degradation, oxidation, and laser ablation during the pump-probe experiment. The sample structure and the experimental geometry is schematically shown in Fig. 1(a). Magnetization dynamics from fs to ns timescales (i.e., from highly nonequilibrium to close-to-equilibrium regime) is measured using time-resolved magneto optical Kerr effect (TR-MOKE) setup based on a two-color, noncollinear, all-optical pump-probe technique. To obtain the intrinsic magnetic response in TR-MOKE, we measure Kerr signals for opposite magnetization directions and take the difference of the two signals to extract the pure magnetic response, whereas the nonmagnetic signal contributions are

obtained as the sum of the two signals [39]. Further details of the measurement technique is provided in the Supplemental Material [40]. In order to calibrate the material properties in the equilibrium regime we study the hysteresis characteristics of the bilayer in the absence of excitation pulse. The in-plane hysteresis loop of the bilayer as shown in Fig. 1(b) is measured by the same MOKE set up by blocking the pump beam. The rectangular shaped hysteresis loop indicates that in static case, the bilayer system behaves as a coupled system with one effective magnetic medium across the total thickness.

The ultrafast demagnetization dynamics of the heterostructure in the highly nonequilibrium regime (typically spanning subpicosecond timescales) caused by excitation by a femtosecond laser pulse is modeled using the temperature-based μT model for bilayers [41,42]. This model traces the temporal evolution of temperatures and chemical potentials for spin-up and spin-down electrons separately for individual layers. The nonequilibrium in the spin-dependent temperatures and chemical potentials caused by laser excitation drives the initial magnetization dynamics. The internal coupling parameters for chemical potential and temperature coupling in the individual materials are obtained from previous experimental measurements for Co [43] and Py [44], respectively. At the interface, spin-resolved particle and energy transfer processes are explicitly taken into account. The spin-resolved electronic temperatures and chemical potentials determine spin-resolved Fermi distributions from which we determine the respective particle numbers of both the spin-up and spin-down reservoirs and thus the magnetization. The particle densities were obtained using the densities of states (DOS) for Co [45] and Py [46]. Both layers are homogeneously excited by the pump laser pulse. We calculate the absorption of the individual layers with the transfer matrix method from the refractive indices for the experimental wavelength of 800 nm. Further details of the model can be found in Ref. [41]. All parameters of the calculation are listed in the Supplemental Material [40].

III. RESULTS AND DISCUSSION

We first study the ultrafast demagnetization and fast remagnetization processes (highly nonequilibrium regime after excitation by fs laser pulses) of the Co (1.5 nm)/Py (1.5 nm) bilayer. We analyze the demagnetization dynamics using experimental methods and theoretical simulations. First, we compare the experimental demagnetization of the Co/Py bilayer to the contributions of the individual Co and Py layers in a coupled bilayer using μT model simulations. Figure 2(a) shows the experimental demagnetization traces of the Co/Py bilayer (solid line) and the theoretically calculated contributions of the Co (short-dashed-lines) and Py (long-dashed-lines) layers at two different excitation fluences. The demagnetization dynamics at lower and higher pump fluences are represented by red ($F = 1.8$ mJ cm^{-2}) and blue ($F = 5.5$ mJ cm^{-2}) lines, respectively. We perform high-resolution time-resolved Kerr rotation experiments for up to 10 ps from the zero delay with a temporal resolution of 30 fs. Our method probes the magnetization dynamics of the entire bilayer system. A rapid decrease of magnetization takes place on the fs timescales, followed by a pronounced recovery. From the calculated demagnetization dynamics of

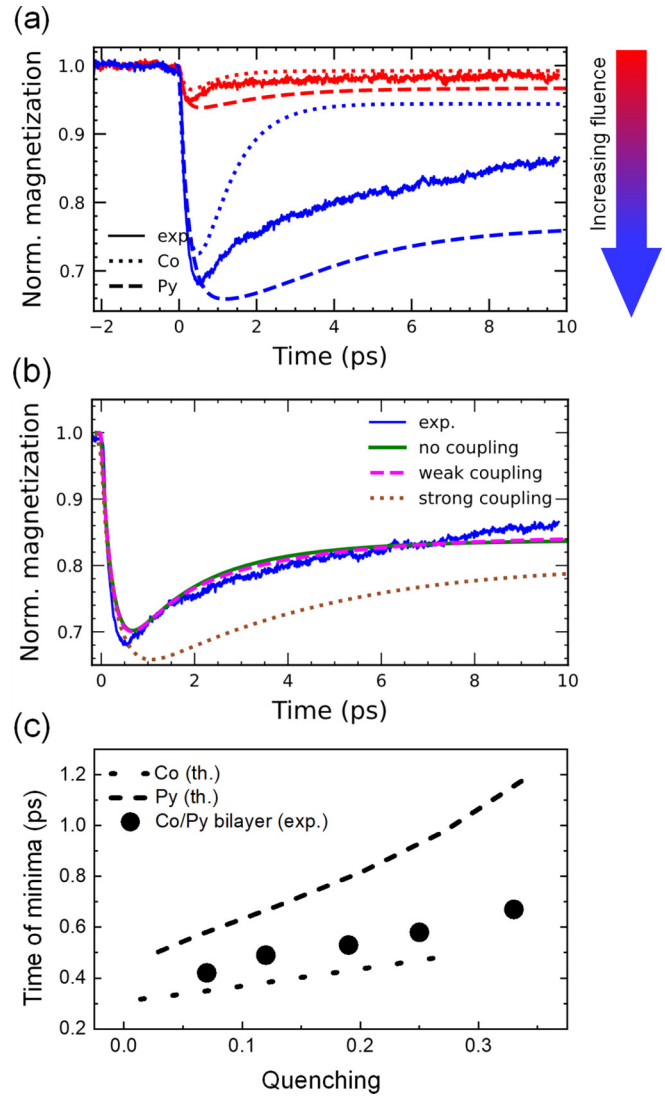


FIG. 2. Comparison of the experimental demagnetization dynamics of the Co/Py bilayer with theoretical μT model. (a) The magnetization curves of the bilayer for one selected low (red) and high (blue) fluence is in between the contributions from the individual layers of the bilayer. (b) Combined theoretical magnetization for various coupling strengths in comparison to the experimental data. (c) The time of minima vs. quenching determined by the fluence for the experimental bilayer and for the individual layers from theory. The results indicate decoupled dynamics at ultrafast timescales (see text).

Fig. 2(a), it is evident that at a particular excitation fluence, Co exhibits faster de- and remagnetization dynamics compared to Py. Such behavior has also been previously observed experimentally [44,47]. However, the experimental demagnetization traces of the Co/Py bilayer lie between those of the individual Co and Py layers. At early timescales, after ultrashort laser pulse excitation, the bilayer exhibits demagnetization dynamics that is faster than that of Py but similar to that of Co. However, the remagnetization dynamics of the bilayer is slower than that of Co and lies between Co and Py. Additionally, we can distinguish the contributions from the individual materials in the simulated remagnetization dynamics

with a fast timescale in the beginning stemming from Co and a slower one later on stemming from Py.

In Fig. 2(b) we combine the numerically simulated demagnetization of the individual Co and Py layers to obtain the demagnetization dynamics of the entire bilayer. This is further compared to the experimentally measured data of the entire bilayer. On ultrafast timescales, we find good agreement with the experimental demagnetization traces for a 3:1 superposition of layer-dependent contributions from the μT model simulations. The simulated magnetization of the bilayer with the parameters used in Fig. 2(a) is denoted as "weak coupling" in Fig. 2(b) (long-dashed magenta line). We call the coupling weak because in the simulations in this case we find only small deviations from the magnetization of completely decoupled Co and Py layers [i.e., in the simulations we consider a bilayer formed of Co and Py layers, but without considering any coupling between the individual layers ("no coupling", solid green line)]. On the other hand, in the simulated case where the coupling between individual Co and Py layers is strong (for example, by increasing the interlayer coupling parameter by a factor of 500), the resulting magnetization deviates significantly from the experimental data ("strong coupling", short-dashed brown line). We conclude that the experimental demagnetization of the bilayer is best described by weakly coupled or decoupled Co and Py layers within the bilayer.

Next, we quantitatively compare the quenching vs. time required to reach the minima for the Co/Py bilayer, and individual Co and Py layers in Fig. 2(c). Here, it is evident that the time required to reach the minima increases steadily with increasing quenching, in line with previous results [5,10,44,48]. This behavior can be attributed to enhanced magnetic fluctuations, which result from a higher population of hot electrons at elevated electron temperatures, particularly when the electron temperature approaches the Curie temperature. Magnetic fluctuations can be linked to spin-flip processes caused by EY scattering, where an excited electron interacts with an impurity/phonon. This interaction alters the probability of the electron occupying a particular spin state, depending on the coupling strength between the electron and the spin system. The observed behavior in Fig. 2(c) can also be explained in terms of chemical potentials. Quenching is determined by the transient equilibration between the spin-dependent chemical potentials following their nonequilibrium caused by the excitation pulse [42]. The higher the absorbed fluence, the further will the spin-dependent chemical potentials be pushed away from each other, and the stronger will be the nonequilibrium that accompanies laser excitation. A stronger nonequilibrium implies longer time required to reach transient equilibration of the chemical potentials [42]. However, it should be noted that the slope of the increase is different for all three parts of the bilayer considered, as shown in Fig. 2(c). The demagnetization is fastest in the Co layer and slowest in the Py layer, whereas the experimentally measured total bilayer exhibits intermediate timescales. The comparison between theory and experiment shows that on ultrafast timescales, during the reduction of magnetic order by the interaction with the ultrashort laser pulse, the dynamics of the individual materials in the bilayer are decoupled from each other. This implies that in the highly nonequilibrium regime (fs timescales), the intrinsic layer-dependent demagnetization processes has a larger influence on the dynamics than the potential interfacial coupling.

We further analyze the demagnetization dynamics using an additional approach. We compare our experimental demagnetization traces with the phenomenological three-temperature model (3TM) [49], which is obtained by solving the energy rate equation between three different degrees of freedom, e.g., electron, spin, and lattice. By considering the specific heats of electron and lattice to be constant and neglecting the specific heat of spin and the electron thermalization time, the following expression can be derived from the 3TM [49]:

$$-\frac{\Delta M}{M} = \Bigg[\Bigg(\frac{A_1}{\sqrt{1+t/\tau_0}} - \frac{A_2\tau_E - A_1\tau_M}{\tau_E - \tau_M}e^{-t/\tau_M} - \frac{\tau_E(A_1 - A_2)}{\tau_E - \tau_M}e^{-t/\tau_E}\Bigg)H(t) + A_3\delta(t)\Bigg] \otimes G(t). \tag{1}$$

Here, τ_M and τ_E are ultrafast demagnetization and fast remagnetization times, respectively. A_1 represents the amplitude of magnetization after equilibrium between the electron, spin, and lattice is restored, A_2 is proportional to the maximum rise in the electronic temperature, and A_3 represents the state-filling or bleaching effects during pump-probe temporal overlap described by a Dirac delta function. $H(t)$ is the Heaviside step function, $\delta(t)$ is the Dirac delta distribution, and $G(t)$ is a Gaussian function that corresponds to the laser pulse. The time constant τ_0 represents the heat diffusion time scale. The TR-MOKE signals of the demagnetization evolution after ultrashort optical excitation measured at different excitation fluences (F) ranging from 1.8 to 8.2 mJ cm^{-2} are shown in Fig. 3(a). The fit reveals an increase in both demagnetization time τ_M and fast remagnetization time τ_E with increasing fluence as shown in Figs. 3(b) and 3(c), respectively. This behavior is in agreement with Fig. 2(b). It is worth mentioning that the values of both τ_M and τ_E for the bilayer are lower than those obtained earlier for the pure Py sample [44].

We next study the precessional magnetization dynamics in the close-to-equilibrium regime well after the laser excitation. The precession dynamics in the GHz range is governed by the phenomenological Landau-Lifshitz-Gilbert (LLG) equation [50]. Figure 4(a) shows the background-subtracted time-resolved precession data for two different magnetic fields, fitted with a damped sinusoidal equation,

$$M(t) = M(0)e^{-t/\tau_d}\sin(2\pi f t), \tag{2}$$

where $M(0)$ is the initial amplitude of the precession, τ_d is the precession relaxation time obtained as a fitting parameter, and f is the precession frequency. The precession frequency can also be extracted directly from the fast Fourier transform (FFT) of the precessional oscillation, which yields a single magnon mode in each case [Fig. 4(b)], indicating that on longer timescales, the individual layers of the bilayer precess together in a coupled way with the same frequency. The observation of coupled behavior is in contrast to some earlier reports [32,33,36,51], where two modes were observed for bilayers with much higher thickness. Previously, Crew *et al.* [32] reported two magnon modes in a thicker bilayer film Py (50 nm)/Co (100 nm) sample, which were termed optical and acoustic modes. Later, Haldar *et al.* [36] observed

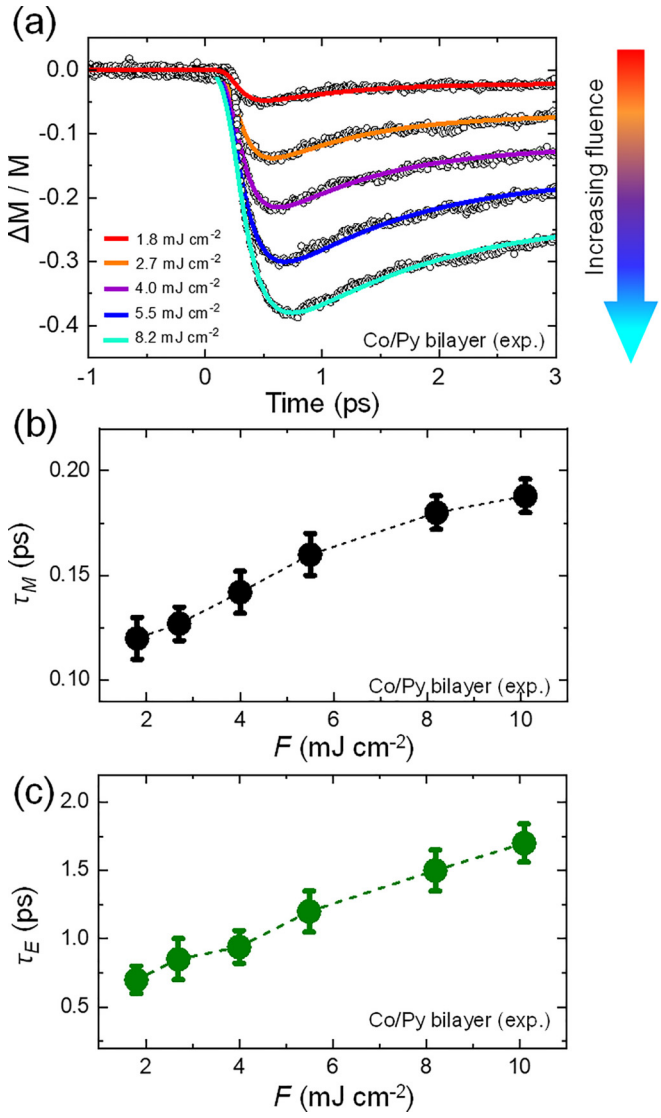


FIG. 3. (a) Ultrafast demagnetization traces of the Co/Py bilayer at different pump fluences (F) fitted with the phenomenological three-temperature model (3TM). Black dots are experimental data and the solid lines of different colors are the fitting lines with the 3TM. Different colors indicate different F values as mentioned in the graph. (b) Demagnetization times τ_M vs F, (c) fast remagnetization times τ_E vs F.

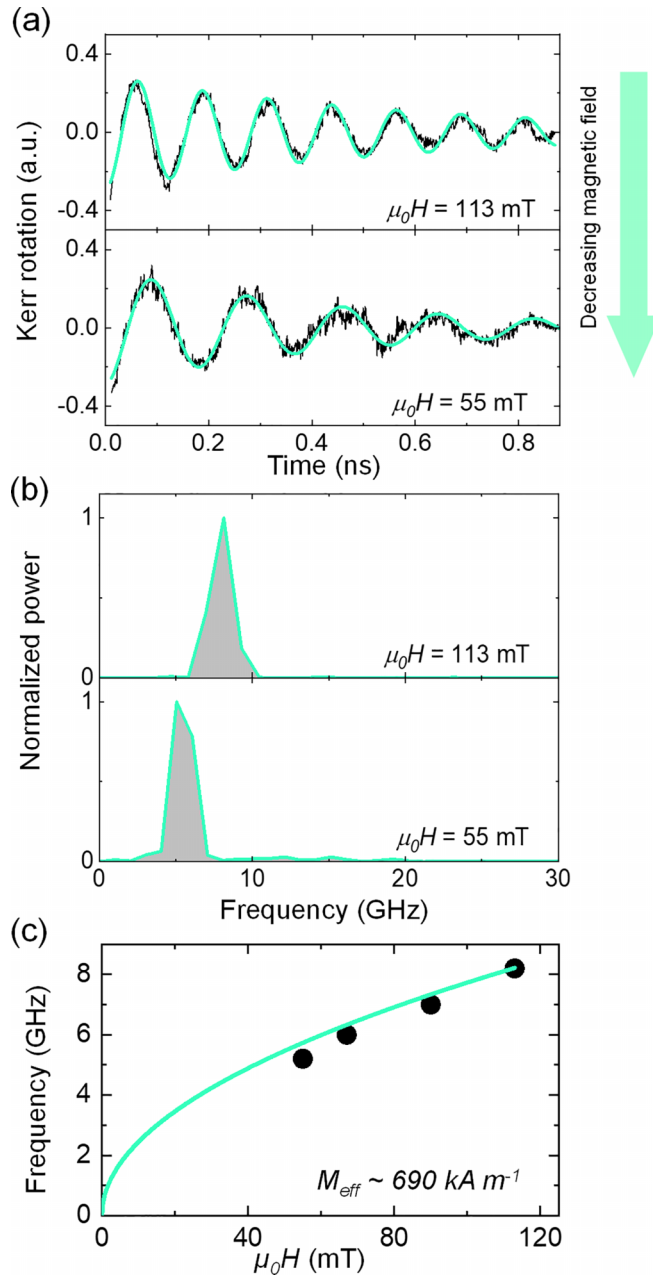


FIG. 4. Magnetic field dependent precession dynamics: (a) Background-subtracted time-resolved Kerr rotation data for the Co/Py bilayer sample measured at three different magnetic fields and at $F = 8.2$ mJ cm^{-2}. Brown solid lines are fitting lines. (b) Corresponding FFT power spectra. (c) Magnetic field dependence of precession frequency. Solid line represent the Kittel fit to the data points.

two modes in much thinner Py (10–30 nm)/Co (10 nm) bilayer system by Brillouin Light scattering technique, which were characterized differently as Damon-Eshbach (DE) and perpendicular standing spin wave (PSSW) modes. The contrasting observations of the magnon dynamics in the literature relative to our work is likely due to the bilayer studied here being much thinner as compared to those studied elsewhere. In ultrathin layers, PSSW mode frequencies are predicted to be $\gtrsim$100 GHz. This is due to the fact that the film thickness becomes much smaller than the spin-wave wavelength, leading to elevated frequencies of these modes. However, the experimental observation of PSSW modes in ultrathin films is very challenging due to their low magneto-optical sensitivity and high damping; these modes rely on spatial confinement across the film's thickness [52]. The effective magnetization M_{eff}, which includes the saturation magnetization and potential additional out-of-plane (OOP) anisotropies, is calculated from the magnetic field dependence of the precession frequencies in Fig. 4(c) and fitting the data points with the Kittel formula [53],

$$f = \frac{1}{2\pi}\sqrt{\omega_{\text{H}}(\omega_{\text{H}} + \omega_{\text{M}})}, \tag{3}$$

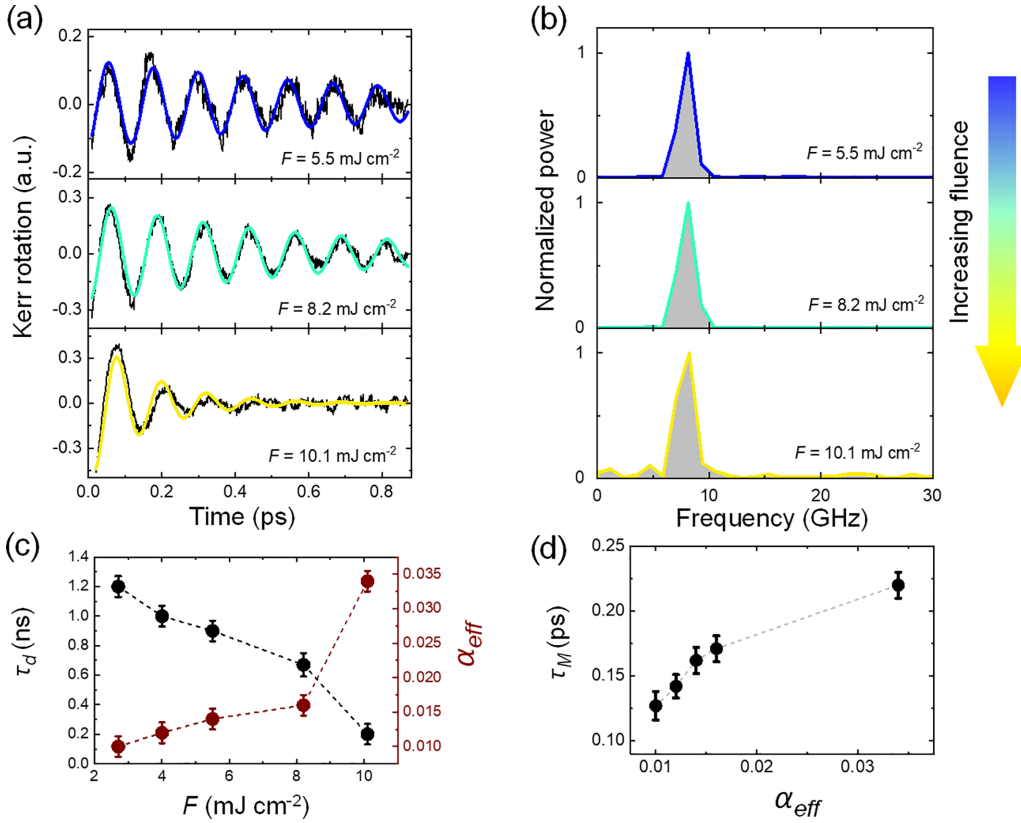


FIG. 5. Pump fluence dependent precession dynamics: (a) Background-subtracted time-resolved Kerr rotation data for the Co/Py bilayer sample measured at different pump fluences (F) and at magnetic fields and at $\mu_0 H = 113$ mT. (b) Corresponding FFT power spectra. (c) Variation of precessional relaxation time τ_d and effective damping α_{eff} with pump fluence. (d) Direct correlation between demagnetization time and effective damping.

where $\omega_H = \gamma \mu_0 H$, $\omega_M = \gamma \mu_0 M_{\text{eff}}$ and H is the externally applied magnetic field and $\gamma = g\mu_B/\hbar$ is the gyromagnetic ratio with g = 2. From the fit, M_{eff} is obtained to be $\sim 690 \pm 20$ kA m^{-1} for the Co/Py bilayer. This value is much smaller than Co ($\sim$1400 kA m^{-1}) and closer to that of Py ($\sim$760 kA m^{-1}) [10,44]. Although the low value of M_{eff} may seem surprising at first, it is not uncommon for ultrathin ferromagnetic layers to have a reduced M_{eff}, which is often due to emerging interfacial anisotropies. However, further extensive research would be needed in future to better understand the precise microscopic origin of the observed precessional frequency and, consequently, the M_{eff} value of the ultrathin bilayer that approximates the Py value in a state of near-equilibrium.

We next study the modulation of precessional dynamics with excitation fluence. Figure 5(a) shows the background-subtracted time-resolved Kerr rotation data of the bilayer measured at different pump fluences (F) and fixed magnetic field $\mu_0 H = 113$ mT. The corresponding FFT power spectra in Fig. 5(b) shows a single precessional mode in each case which again indicates that on longer timescales the two layers precess together in a coupled way with the same frequency. It is worth mentioning that, in contrast to our earlier work on Ni [54], here we do not observe any significant phase shift of the precessional dynamics with pump fluence. This is an indication of weak magnetoelastic (ME) coupling in this sample. We can calculate the effective damping factor α_{eff} from the extracted value of precessional relaxation time τ_d and M_{eff} as [10,17,44]

$$\alpha_{\text{eff}} = \frac{1}{\tau_d\left(\omega_H + \frac{\omega_M}{2}\right)}. \tag{4}$$

Figure 5(c) shows an enhancement in α_{eff} associated with a corresponding decrease in the precessional relaxation time τ_d as the pump fluence (F) increases. We observe that α_{eff} increases from 0.010 to 0.035 as F increases from 2.7 to 10.1 mJ cm^{-2}. Various procedures for exciting long time scale (ns) precessional (magnon) dynamics show different mechanisms responsible for the exploration of different energy and angular momentum transfer channels. Microscopically, the EY spin-phonon interaction mechanism has been thought to be the main contribution to precessional damping [20,52,55]. Phenomenological models suggest that as fluence increases, the transient rise in the ratio of the system temperature to the Curie temperature exerts an influence on magnetization relaxation via susceptibility, resulting in higher damping [52,56,57]. This aligns with the quantum Landau-Lifshitz-Bloch (LLB)-based model of Nieves *et al.* [58] which links damping to temperature via spin-flip scattering mechanisms. Moreover, the transient rise of system temperature at higher pump fluences in turn increases the probability of generation

of more incoherent (or thermal) magnons relative to coherent magnons leading to dephasing driven by nonlinear magnon-magnon interactions at elevated temperature [44]. Hence, we observe some nonlinearities in α_{eff} at high pump fluences.

Finally, we turn to the direct correlation observed between demagnetization time τ_{M} and effective damping α_{eff}, illustrated in Fig. 5(d). The relationship between ultrafast demagnetization and effective damping serves as a sensitive indicator of interconnected microscopic pathways for angular momentum transfer in ferromagnets [9,10,20,29,55]. Both processes require the transfer of angular momentum from the spin system to the lattice via spin-flip scattering following laser excitation. In 2005, Koopmans *et al.* [9] predicted, on the basis of quantum-mechanical arguments, an inverse proportionality between demagnetization time and damping. This model, however, prompted considerable debate, as experiments tuning these quantities via transition-metal and rare-earth doping failed to confirm the predicted relationship [17]. In 2010, Fähnle *et al.* [20] showed that damping can be either directly or inversely proportional to τ_{M}, depending on whether damping is dominated by conductivity-like intraband scattering ("breathing Fermi surface") or resistivity-like interband scattering, respectively. In a follow-up study, they later noted that spin transport must also be considered [29]: while nonlocal spin transport can significantly shorten τ_{M}, spin-pumping-induced spin currents can enhance Gilbert damping. Thus, even in a conductivity-like regime, a direct demagnetization time-damping relationship occurs only when local spin-flip scattering dominates demagnetization, whereas an inverse relationship indicates nonlocal spin transport as the prevailing microscopic mechanism.

Here, we investigate the τ_{M}-α_{eff} correlation in an ultrathin Co/Py bilayer by systematically varying the excitation fluence, extending earlier studies on single-layer ferromagnetic films [10]. It is important to keep in mind that we are comparing the dynamics of a decoupled system on fs timescales with those of a coupled system on ns timescales. At lower fluences, τ_{M} and the effective damping α_{eff} scale directly [Fig. 5(d)], consistent with a conductivity-like regime dominated by localized spin-flip scattering. This direct relationship is also consistent with that observed by Fähnle *et al.* for Co/Ni bilayers as a function of increasing Ni layer thickness [20]. In our case, the increase of τ_{M} with fluence [as shown in Fig. 3(b)] can be understood as a general feature of Elliott–Yafet-type scattering, where stronger quenching necessitates more spin-flip events to transfer angular momentum to the lattice [5,10,44,48,59–61], or as a consequence of a greater separation of spin-dependent chemical potentials, which further slows demagnetization [42]. On nanosecond timescales, α_{eff} also increases with fluence [Fig. 5(c)], which is attributed to a transient rise in the system-to-Curie-temperature ratio, enhancing magnon excitation [44,52,56–58]. This linear increase in both demagnetization time and effective damping as a function of excitation fluence results in the direct relationship observed between τ_{M} and α_{eff}, but only when local spin-flip scattering dominates demagnetization. However, as discussed above, nonlinear effects of the magnon system set in at higher fluences, resulting in a slight deviation from the linear τ_{M}-α_{eff} trend, as observed at the final point in Fig. 5(d).

IV. SUMMARY AND CONCLUSION

In summary, we have studied the magnetization dynamics of an ultrathin Co (1.5 nm)/Py (1.5 nm) bilayer from femtosecond (fs) to nanosecond (ns) timescales. We observe that the interfacial effects in such bilayer is dynamic (i.e., timescale dependent). On fs timescales, the dynamics indicate that the constituent layers of the bilayer behave decoupled from each other when the system is in a highly nonequilibrium regime caused by ultrashort laser excitation. However, on longer (ns) timescales, when the system is in close to equilibrium, the individual layers of the bilayer precess together as an effective single layer in a coupled manner with a single frequency. Furthermore, the direct proportionality or direct correlation observed between demagnetization time and effective damping in the bilayer points to the possible involvement of local Elliott-Yafet spin-flip scattering as a contributing mechanism in the ultrafast magnetization dynamics of the system. Since both demagnetization time and damping require a transfer of angular momentum from the electronic system to the lattice, the unification of these two seemingly unrelated parameters can facilitate the exploration of the microscopic mechanism of laser-induced magnetization dynamics from femtosecond to nanosecond timescales. Such a detailed analysis of different nonequilibrium regimes of magnetization dynamics and the attempt to find a bridge between them in an exchange coupled, epitaxially grown Co/Py ultrathin bilayer will expedite its use in technological applications.

ACKNOWLEDGMENTS

The authors are thankful to B. Hillebrands, H. C. Schneider, and B. Stadtmüller for helpful discussion. The authors appreciate the Allianz für Hochleistungsrechnen Rheinland-Pfalz for providing computing resources on the Elwetritsch high-performance computing cluster. The authors gratefully acknowledge financial support of the Deutsche Forschungsgemeinschaft (DFG, German Research Foundation) through the SFB/TRR-173-268565370 "Spin + X" (projects A08, B03, and B11). A.D. further acknowledges TU-Nachwuchsring, RPTU Kaiserslautern-Landau for research funding.

A.D. and C.S. contributed equally. A.D., P.H., and A.L. designed and performed TR-MOKE experiments. A.D. analyzed the experimental results in consultation with M.A., G.v.F., P.P., and L.S. fabricated the sample. C.S. performed μT-model simulations in consultation with B.R., and S.A. All authors contributed to the analysis and discussion for the results. A.D., C.S., and S.A. wrote the first draft of the manuscript. All authors contributed to the editing of the manuscript.

DATA AVAILABILITY

The data that support the findings of this article are not publicly available upon publication because it is not technically feasible and/or the cost of preparing, depositing, and hosting the data would be prohibitive within the terms of this research project. The data are available from the authors upon reasonable request.

[1] E. Beaurepaire, J.-C. Merle, A. Daunois, and J.-Y. Bigot, Ultrafast spin dynamics in ferromagnetic nickel, Phys. Rev. Lett. **76**, 4250 (1996).

[2] B. Koopmans, M. van Kampen, J. T. Kohlhepp, and W. J. M. de Jonge, Ultrafast magneto-optics in nickel: Magnetism or optics?, Phys. Rev. Lett. **85**, 844 (2000).

[3] J.-Y. Bigot, M. Vomir, and E. Beaurepaire, Coherent ultrafast magnetism induced by femtosecond laser pulses, Nat. Phys. **5**, 515 (2009).

[4] M. Krauß, T. Roth, S. Alebrand, D. Steil, M. Cinchetti, M. Aeschlimann, and H. C. Schneider, Ultrafast demagnetization of ferromagnetic transition metals: The role of the Coulomb interaction, Phys. Rev. B **80**, 180407(R) (2009).

[5] B. Koopmans, F. D. Longa, G. Malinowski, D. Steiauf, M. Fähnle, T. Roth, M. Cinchetti, and M. Aeschlimann, Explaining the paradoxical diversity of ultrafast laser-induced demagnetization, Nat. Mater. **9**, 259 (2010).

[6] G. Malinowski, F. D. Longa, J. H. H. Rietjens, P. V. Paluskar, R. Huijink, H. J. M. Swagten, and B. Koopmans, Control of speed and efficiency of ultrafast demagnetization by direct transfer of spin angular momentum, Nat. Phys. **4**, 855 (2008).

[7] M. Battiato, K. Carva, and P. M. Oppeneer, Superdiffusive spin transport as a mechanism of ultrafast demagnetization, Phys. Rev. Lett. **105**, 027203 (2010).

[8] M. van Kampen, C. Jozsa, J. T. Kohlhepp, P. LeClair, L. Lagae, W. J. M. de Jonge, and B. Koopmans, All-optical probe of coherent spin waves, Phys. Rev. Lett. **88**, 227201 (2002).

[9] B. Koopmans, J. J. M. Ruigrok, F. Longa, and W. J. M. de Jonge, Unifying ultrafast magnetization dynamics, Phys. Rev. Lett. **95**, 267207 (2005).

[10] S. Mukhopadhyay, S. Majumder, S. N. Panda, and A. Barman, Investigation of ultrafast demagnetization and Gilbert damping and their correlation in different ferromagnetic thin films grown under identical conditions, Nanotechnology **34**, 235702 (2023).

[11] S. Ashok, J. Hoefer, M. Stiehl, M. Aeschlimann, H. Christian Schneider, B. Rethfeld, and B. Stadtmüller, Signatures of ballistic and diffusive transport in the time-dependent Kerr-response of magnetic materials, New J. Phys. **27**, 063001 (2025).

[12] A. De, K. Dutta, S. Mondal, S. Barman, Y. Otani, and A. Barman, Magnonic crystals with complex geometry, Phys. Rev. B **103**, 064402 (2021).

[13] A. De, S. S. P. K. Arekapudi, L. Koch, F. Samad, S. N. Panda, B. Böhm, O. Hellwig, and A. Barman, Magnetic configuration driven femtosecond spin dynamics in synthetic antiferromagnets, ACS Appl. Mater. Interf. **14**, 13970 (2022).

[14] G. P. Zhang, W. Hübner, G. Lefkidis, Y. Bai, and T. F. George, Paradigm of the time-resolved magneto-optical Kerr effect for femtosecond magnetism, Nat. Phys. **5**, 499 (2009).

[15] S. Ashok, C. Seibel, S. T. Weber, J. Briones, and B. Rethfeld, Influence of diffusive transport on ultrafast magnetization dynamics, Appl. Phys. Lett. **120**, 142402 (2022).

[16] G. P. Zhang and W. Hübner, Laser-induced ultrafast demagnetization in ferromagnetic metals, Phys. Rev. Lett. **85**, 3025 (2000).

[17] J. Walowski, G. Müller, M. Djordjevic, M. Münzenberg, M. Kläui, C. A. F. Vaz, and J. A. C. Bland, Energy equilibration processes of electrons, magnons, and phonons at the femtosecond time scale, Phys. Rev. Lett. **101**, 237401 (2008).

[18] M. Vomir, L. H. F. Andrade, L. Guidoni, E. Beaurepaire, and J.-Y. Bigot, Real space trajectory of the ultrafast magnetization dynamics in ferromagnetic metals, Phys. Rev. Lett. **94**, 237601 (2005).

[19] F. Dusabirane, K. Leckron, B. Rethfeld, and H. C. Schneider, Interplay of electron-magnon scattering and spin-orbit induced electronic spin-flip scattering in a two-band Stoner model, arXiv:2304.14978.

[20] M. Fähnle, J. Seib, and C. Illg, Relating Gilbert damping and ultrafast laser-induced demagnetization, Phys. Rev. B **82**, 144405 (2010).

[21] W. Zhang, Q. Liu, Z. Yuan, K. Xia, W. He, Q.-F. Zhan, X.-Q. Zhang, and Z.-H. Cheng, Enhancement of ultrafast demagnetization rate and Gilbert damping driven by femtosecond laser-induced spin currents in $Fe_{81}Ga_{19}/Ir_{20}Mn_{80}$ bilayers, Phys. Rev. B **100**, 104412 (2019).

[22] S. Mukhopadhyay, P. K. Pal, S. Manna, C. Mitra, and A. Barman, Laser fluence tunable spin transport and ultrafast demagnetization in $BiSbTe_{1.5}Se_{1.5}/Co_{20}Fe_{60}B_{20}$ bilayers, Phys. Rev. B **109**, 024437 (2024).

[23] M. Aeschlimann, A. Vaterlaus, M. Lutz, M. Stampanoni, and F. Meier, Ultrafast thermomagnetic writing processes in rare-earth transition-metal thin films, J. Appl. Phys. **67**, 4438 (1990).

[24] I. Radu, K. Vahaplar, C. Stamm, T. Kachel, N. Pontius, H. A. Dürr, T. A. Ostler, J. Barker, R. F. L. Evans, R. W. Chantrell, A. Tsukamoto, A. Itohm, A. Kirilyuk, T. Rasing, and A. V. Kimel, Transient ferromagnetic-like state mediating ultrafast reversal of antiferromagnetically coupled spins, Nature (London) **472**, 205 (2011).

[25] R. Medapalli, I. Razdolski, M. Savoini, A. R. Khorsand, A. Kirilyuk, A. V. Kimel, T. Rasing, A. M. Kalashnikova, A. Tsukamoto, and A. Itoh, Efficiency of ultrafast laser-induced demagnetization in $Gd_xFe_{100-x-y}Co_y$ alloys, Phys. Rev. B **86**, 054442 (2012).

[26] V. López-Flores, N. Bergeard, V. Halté, C. Stamm, N. Pontius, M. Hehn, E. Otero, E. Beaurepaire, and C. Boeglin, Role of critical spin fluctuations in ultrafast demagnetization of transition-metal rare-earth alloys, Phys. Rev. B **87**, 214412 (2013).

[27] M. J. G. Peeters, Y. M. van Ballegooie, and B. Koopmans, Influence of magnetic fields on ultrafast laser-induced switching dynamics in Co/Gd bilayers, Phys. Rev. B **105**, 014429 (2022).

[28] B. Liu, H. Xiao, and M. Weinelt, Microscopic insights to spin transport–driven ultrafast magnetization dynamics in a Gd/Fe bilayer, Sci. Adv. **9**, eade0286 (2023).

[29] W. Zhang, W. He, X.-Q. Zhang, Z.-H. Cheng, J. Teng, and M. Fähnle, Unifying ultrafast demagnetization and intrinsic Gilbert damping in Co/Ni bilayers with electronic relaxation near the Fermi surface, Phys. Rev. B **96**, 220415(R) (2017).

[30] E. Kneller and R. Hawig, The exchange-spring magnet: A new material principle for permanent magnets, IEEE Trans. Magn. **27**, 3588 (1991).

[31] E. E. Fullerton, J. S. Jiang, M. Grimsditch, C. H. Sowers, and S. D. Bader, Exchange-spring behavior in epitaxial hard/soft magnetic bilayers, Phys. Rev. B **58**, 12193 (1998).

[32] D. C. Crew, K. J. Kennewell, M. J. Lwin, R. C. Woodward, S. Prasad, and R. L. Stamps, Optic and acoustic modes measured in a cobalt/permalloy exchange spring bilayer using inductive magnetometry, J. Appl. Phys. **97**, 10A707 (2005).

[33] K. J. Kennewell, M. Kostylev, N. Ross, R. Magaraggia, R. L. Stamps, M. Ali, A. A. Stashkevich, D. Greig, and B. J. Hickey, Magnetization pinning at a Py/Co interface measured using broadband inductive magnetometry, J. Appl. Phys. **108**, 073917 (2010).

[34] J. Deng, A. Tan, J. Li, C. Hwang, and Z. Q. Qiu, In-plane spin reorientation transition in Co/Py bilayers grown epitaxially on vicinal Cu(001), J. Magn. Magn. Mater. **408**, 193 (2016).

[35] A. Fraile Rodríguez, L. J. Heyderman, F. Nolting, A. Hoffmann, J. E. Pearson, L. M. Doeswijk, M. A. F. van den Boogaart, and J. Brugger, Permalloy thin films exchange coupled to arrays of cobalt islands, Appl. Phys. Lett. **89**, 142508 (2006).

[36] A. Haldar, C. Banerjee, P. Laha, and A. Barman, Brillouin light scattering study of spin waves in NiFe/Co exchange spring bilayer films, J. Appl. Phys. **115**, 133901 (2014).

[37] M. Salaheldeen, L. Martínez-Goyeneche, P. Alvarez-Alonso, and A. Fernández, Formation of Néel-type skyrmions in an antidot lattice with perpendicular magnetic anisotropy, Nanotechnology **31**, 485708 (2020).

[38] T. Feggeler, R. Meckenstock, D. Spoddig, C. Schöppner, B. Zingsem, T. Schaffers, H. Ohldag, H. Wende, M. Farle, A. Ney, and K. Ollefs, Element-specific visualization of dynamic magnetic coupling in a Co/Py bilayer microstructure, Sci. Rep. **12**, 18724 (2022).

[39] R. Wilks, R. J. Hicken, M. Ali, B. J. Hickey, J. D. R. Buchanan, A. T. G. Pym, and B. K. Tanner, Investigation of ultrafast demagnetization and cubic optical nonlinearity of Ni in the polar geometry, J. Appl. Phys. **95**, 7441 (2004).

[40] See Supplemental Material at http://link.aps.org/supplemental/10.1103/d7vt-jlkg for S1. Time-resolved MOKE experiments, S2. μT model for bilayers, and S3. Transient temperature rise using μT model, which includes Refs. [8,39,41,42,62–65].

[41] C. Seibel, M. Weber, M. Stiehl, S. T. Weber, M. Aeschlimann, H. C. Schneider, B. Stadtmüller, and B. Rethfeld, Control of transport phenomena in magnetic heterostructures by wavelength modulation, Phys. Rev. B **106**, L140405 (2022).

[42] B. Y. Mueller and B. Rethfeld, Thermodynamic μ T model of ultrafast magnetization dynamics, Phys. Rev. B **90**, 144420 (2014).

[43] D. Zusin, P. M. Tengdin, M. Gopalakrishnan, C. Gentry, A. Blonsky, M. Gerrity, D. Legut, J. M. Shaw, H. T. Nembach, T. J. Silva, P. M. Oppeneer, H. C. Kapteyn, and M. M. Murnane, Direct measurement of the static and transient magneto-optical permittivity of cobalt across the entire M-edge in reflection geometry by use of polarization scanning, Phys. Rev. B **97**, 024433 (2018).

[44] A. De, A. Lentfert, L. Scheuer, B. Stadtmüller, G. von Freymann, M. Aeschlimann, and P. Pirro, Coherent and incoherent magnons induced by strong ultrafast demagnetization in thin permalloy films, Phys. Rev. B **109**, 024422 (2024).

[45] F. Batallan, I. Rosenman, and C. Sommers, Band structure and Fermi surface of hcp ferromagnetic cobalt, Phys. Rev. B **11**, 545 (1975).

[46] M. He, C. Wu, M. V. Shugaev, G. D. Samolyuk, and L. V. Zhigilei, Computational study of short-pulse laser-induced generation of crystal defects in Ni-based single-phase binary solid–solution alloys, J. Phys. Chem. C **123**, 2202 (2019).

[47] V. Unikandanunni, R. Medapalli, E. E. Fullerton, K. Carva, P. M. Oppeneer, and S. Bonetti, Anisotropic ultrafast spin dynamics in epitaxial cobalt, Appl. Phys. Lett. **118**, 232404 (2021).

[48] T. Roth, A. J. Schellekens, S. Alebrand, O. Schmitt, D. Steil, B. Koopmans, M. Cinchetti, and M. Aeschlimann, Temperature dependence of laser-induced demagnetization in Ni: A key for identifying the underlying mechanism, Phys. Rev. X **2**, 021006 (2012).

[49] F. Dalla Longa, J. T. Kohlhepp, W. J. M. De Jonge, and B. Koopmans, Influence of photon angular momentum on ultrafast demagnetization in nickel, Phys. Rev. B **75**, 224431 (2007).

[50] T. Gilbert, A phenomenological theory of damping in ferromagnetic materials, IEEE Trans. Magn. **40**, 3443 (2004).

[51] G. B. G. Stenning, L. R. Shelford, S. A. Cavill, F. Hoffmann, M. Haertinger, T. Hesjedal, G. Woltersdorf, G. J. Bowden, S. A. Gregory, and C. H. Back, Magnetization dynamics in an exchange-coupled NiFe/CoFe bilayer studied by x-ray detected ferromagnetic resonance, New J. Phys. **17**, 013019 (2015).

[52] S. Mondal and A. Barman, Laser controlled spin dynamics of ferromagnetic thin film from femtosecond to nanosecond timescale, Phys. Rev. Appl. **10**, 054037 (2018).

[53] C. Kittel, On the theory of ferromagnetic resonance absorption, Phys. Rev. **73**, 155 (1948).

[54] A. Lentfert, A. De, L. Scheuer, B. Stadtmüller, G. von Freymann, M. Aeschlimann, and P. Pirro, Phase shift of coherent magnetization dynamics after ultrafast demagnetization in strongly quenched nickel thin films, J. Phys.: Condens. Matter **36**, 455801 (2024).

[55] K. Gilmore, Y. U. Idzerda, and M. D. Stiles, Identification of the dominant precession-damping mechanism in Fe, Co, and Ni by first-principles calculations, Phys. Rev. Lett. **99**, 027204 (2007).

[56] B. Liu, X. Ruan, Z. Wu, H. Tu, J. Du, J. Wu, X. Lu, L. He, R. Zhang, and Y. Xu, Transient enhancement of magnetization damping in CoFeB film via pulsed laser excitation, Appl. Phys. Lett. **109**, 042401 (2016).

[57] Y. Zhao, Q. Song, S.-H. Yang, T. Su, W. Yuan, S. S. P. Parkin, J. Shi, and W. Han, Experimental investigation of temperature-dependent Gilbert damping in permalloy thin films, Sci. Rep. **6**, 22890 (2016).

[58] P. Nieves, D. Serantes, U. Atxitia, and O. Chubykalo-Fesenko, Quantum Landau-Lifshitz-Bloch equation and its comparison with the classical case, Phys. Rev. B **90**, 104428 (2014).

[59] M. Cinchetti, M. Sánchez Albaneda, D. Hoffmann, T. Roth, J.-P. Wüstenberg, M. Krauß, O. Andreyev, H. C. Schneider, M. Bauer, and M. Aeschlimann, Spin-flip processes and ultrafast magnetization dynamics in Co: Unifying the microscopic and macroscopic view of femtosecond magnetism, Phys. Rev. Lett. **97**, 177201 (2006).

[60] U. Atxitia, O. Chubykalo-Fesenko, J. Walowski, A. Mann, and M. Münzenberg, Evidence for thermal mechanisms in laser-induced femtosecond spin dynamics, Phys. Rev. B **81**, 174401 (2010).

[61] K. C. Kuiper, T. Roth, A. J. Schellekens, O. Schmitt, B. Koopmans, M. Cinchetti, and M. Aeschlimann, Spin-orbit enhanced demagnetization rate in Co/Pt-multilayers, Appl. Phys. Lett. **105**, 202402 (2014).

[62] B. Y. Mueller, T. Roth, M. Cinchetti, M. Aeschlimann, and B. Rethfeld, Driving force of ultrafast magnetization dynamics, New J. Phys. **13**, 123010 (2011).

[63] M. O. A. Ellis, T. A. Ostler, and R. W. Chantrell, Classical spin model of the relaxation dynamics of rare-earth doped permalloy, Phys. Rev. B **86**, 174418 (2012).

[64] P. B. Johnson and R. W. Christy, Optical constants of transition metals: Ti, V, Cr, Mn, Fe, Co, Ni, and Pd, Phys. Rev. B **9**, 5056 (1974).

[65] K. K. Tikuišis, L. Beran, P. Cejpek, K. Uhlířová, J. Hamrle, M. Vaňatka, M. Urbánek, and M. Veis, Optical and magneto-optical properties of permalloy thin films in 0.7–6.4 eV photon energy range, Mater. Des. **114**, 31 (2017).